DESIGN AND ULTRASONIC CHARACTERIZATION OF A THIN-FILM, FLEXIBLE, PMUT ARRAY

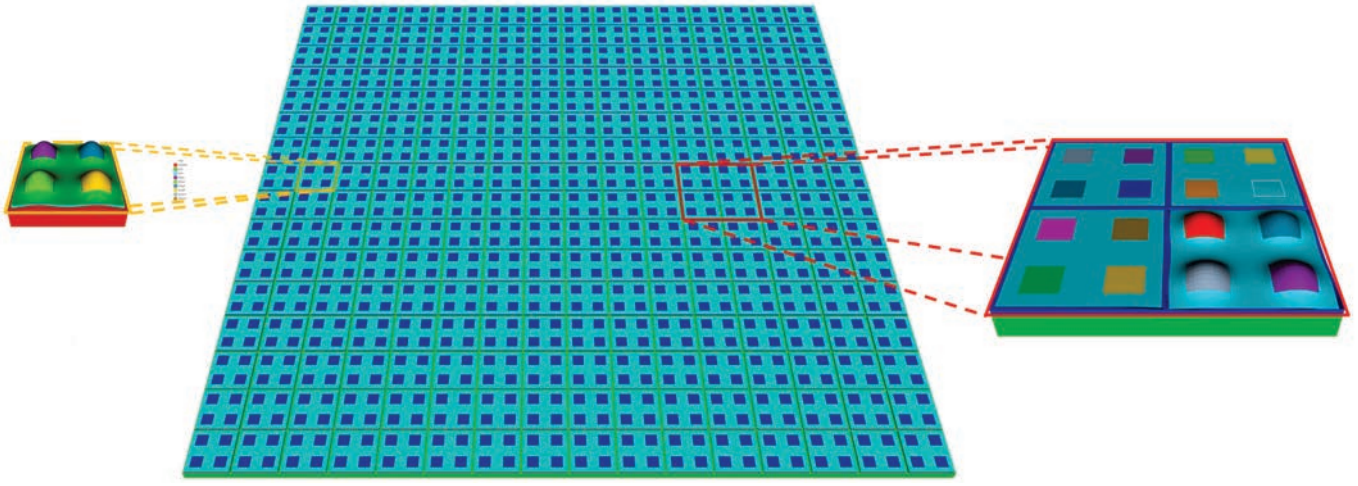

*Jeong Nyeon Kim, Tianning Liu, Thomas N. Jackson, Kyusun Choi, Susan Trolier-McKinstry, Richard L. Tutwiler, and Judith A. Todd, FASM**
The Pennsylvania State University, University Park

A materials and design optimization study uses finite element analyses to improve designs for robust and practical piezoelectric micromachined ultrasonic transducer (PMUT) sensor arrays.

**Member of ASM International*

Ultrasound is widely used for nondestructive evaluation (NDE), structural health monitoring (SHM), acoustic emission, sound navigation ranging, and in sensors for automobiles, medicine, and many other applications. Ultrasound fingerprint sensors[1,2] for user authentication and ultrasound buttons[3,4] are now replacing mechanical buttons. These next-generation, small-form-factor sensors, a few cm^2 or even smaller than 10 mm^2, have been achieved through advances in piezoelectric micromachined ultrasonic transducers (PMUTs) that can be positioned on either a flexible polymer or a silicon substrate to form an array[5-8]. In particular, flexible array sensors can be applied to complex geometries for NDE and SHM, the human body[9], and for medical monitoring and assistive devices[10,11]. Kim et al.[8] have recently shown how finite-element analysis (FEA) can be applied to develop an optimized, robust design of a 10 MHz, flexible, PMUT array sensor. This article presents an improved PMUT array sensor design for a higher resonance frequency of 38 MHz.

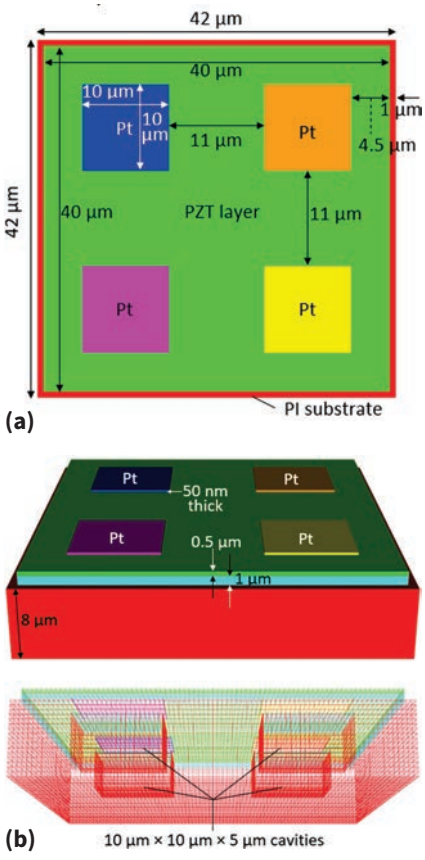

Fig. 1 — The quad diaphragm PMUT cell in (a) planar view with key dimensions and materials, and (b) top and bottom angle views with thickness and cavity dimensions.

PMUT MODEL

Piezoelectric micromachined ultrasonic transducers (PMUTs) have a typical structure of, from the top, a top electrode, $PbZr_{0.52}Ti_{0.48}O_3$ (PZT) active layer, bottom electrode, elastic passive layer, a cavity wrapped by a substrate, and a substrate. The d31 coefficient of PZT leads to stretching and contraction in the radial and/or width directions, depending on its shape, when activated by top and bottom electrodes. The PZT motions impose bending moments on the coupled elastic passive layer so that the diaphragm creates and propagates acoustic waves in the surrounding medium. When the returning acoustic waves hit and bend the diaphragm, the PZT layer experiences mechanical stress and outputs an electric potential via the piezoelectric effect. The flexible PMUT model described in this article was designed to have a resonance frequency close to 40 MHz. It had a quad diaphragm structure—a single PMUT cell with four moving diaphragms. Each diaphragm had 10 × 10 µm planar dimensions, and consisted of, from the top, concentric layers of 50 nm thick platinum (Pt) top electrode/1 µm thick PZT active layer/50 nm thick Pt bottom electrode/1 µm thick titanium (Ti) passive layer/5 µm deep cavity surrounded by a polyimide (PI) substrate. Figure 1 shows schematics of the single PMUT cell model with dimensions, and Table 1 displays dimensions and materials for corresponding modules.

FINITE ELEMENT ANALYSIS MODELING

PZT 8 and materials with the properties shown in Fig. 2 and Table 2 were used for this FEA study[12,13]. It should be noted that full characterization of the elastic and piezoelectric properties of PZT thin films has not yet been achieved. Moreover, the properties of a PZT thin film may change during the complex microfabrication process. Consequently, the original properties

TABLE 1 – MATERIALS AND DIMENSIONS FOR MODULES IN THE QUAD DIAPHRAGM PMUT CELL MODEL

Stack from top			
	Materials and modules	Length × width	Thickness
	Pt top-electrodes	10 µm × 10 µm	50 µm
	Thin-film PZT active layer	40 µm × 40 µm	0.5 µm
Not seen	Pt bottom-electrode	10 µm × 10 µm	100 µm
	Ti passive layer	10 µm × 10 µm	1 µm
	Vacuum cavity	10 µm × 10 µm	5 µm
	PI substrate	42 µm × 42 µm	8 µm

TABLE 2 – MECHANICAL AND DAMPING PROPERTIES OF THE 40 MHz QUAD DIAPHRAGM PMUT MODEL

Material	Mechanical			Damping (viscoelastic)	
	Density	Bulk velocity	Shear velocity	Bulk attenuation	Shear attenuation
Polyimide	1082 kg/m^3	3500 m/s	2000 m/s	9 dB/cm at 10 MHz	13 dB/cm at 10 MHz
Titanium	4480 kg/m^3	6100 m/s	3100 m/s	0.3 dB/MHz/cm	1.2 dB/MHz/cm
Platinum	21,400 kg/m^3	3260 m/s	1730 m/s	0.3 dB/MHz/cm	0.9 dB/MHz/cm

merely provide a starting point for predicting performance of the fabricated devices[14].

Validation of the fundamental resonance frequency can be achieved through electrical input impedance modeling. The single PMUT cell model was driven by a bipolar peak-to-peak voltage, 3 Vpp, and 1 MHz to 500 MHz sinusoidal signal to ensure that the lowest resonance frequency was discovered. The modeling assumed a vacuum environment for calculation efficiency. Figure 3 displays a snapshot of the diaphragm deflections at their centers in the PMUT model simulation. Figure 4 shows the electrical input impedance responses of the four diaphragms in the PMUT cell.

Figure 3 shows the deflections of the respective diaphragm cross-sections, which were coincident. In Fig. 4, all four diaphragms had the same electrical input impedance response. The fundamental resonance and anti-resonance frequencies were found at 39.1 MHz and 40.3 MHz, respectively, satisfying a targeted resonance frequency range near 40 MHz.

A water load was added above the PMUT cell so that the basic characteristics of the PMUT cell, center frequency and bandwidth, could be simulated for the same environment as for water immersion experiments. Figure 5 revealed the center frequency and -6 dB bandwidth of the PMUT water model to be 37.6 MHz and {(44.8-32.7) ÷ 37.6) × 100 %} = 32.3 %, respectively. The model was driven by a bipolar peak-to-peak 3 Vpp, single cycle sine wave. The decreased center frequency, 37.6 MHz from 39.1 MHz, can be explained by the mass loading effect of the water on the diaphragms. The 32.3% bandwidth was relatively narrow for an imaging transducer, a feature that has been addressed by Kim et al.[8], who found that the bandwidth narrowed as the number of PMUT cells increased in a flexible polymer substrate PMUT array. This article addressed increasing the bandwidth beyond that considered by Kim et al.[8].

Piezoelectric coupling matrix of PZT 8 [C/m^2]

$$[e]=\begin{bmatrix} 0 & 0 & 0 & 0 & 12.7 & 0 \\ 0 & 0 & 0 & 12.7 & 0 & 0 \\ -5.2 & -5.2 & 15.08 & 0 & 0 & 0 \end{bmatrix}$$

Stiffness matrix of the thin-film PZT (PZT 8) [N/m^2]

$$[c]=\begin{bmatrix} 1.39\times10^{11} & 7.8\times10^{10} & 7.43\times10^{10} & 0 & 0 & 0 \\ 7.8\times10^{10} & 1.39\times10^{11} & 7.43\times10^{10} & 0 & 0 & 0 \\ 7.43\times10^{10} & 7.43\times10^{10} & 1.154\times10^{11} & 0 & 0 & 0 \\ 0 & 0 & 0 & 2.65\times10^{10} & 0 & 0 \\ 0 & 0 & 0 & 0 & 2.65\times10^{10} & 0 \\ 0 & 0 & 0 & 0 & 0 & 3.06\times10^{10} \end{bmatrix}$$

Relative permittivity, density, and poling direction of PZT 8

ε_{11}	ε_{22}	ε_{33}	Density	Poling direction
900	900	600	7600 kg/m^3	Positive Z

Fig. 2 — Properties of PZT 8 applied to model thin-film PZT.

RESULTS

A 2D, 32x32 array model, comprised of 256 (16×16) quad diaphragm PMUT cells and 1024 (32×32) moving diaphragms, is now considered, as shown in Fig. 6. The 1024 (32×32) moving diaphragms each have the same kerf, 11 µm, and the same pitch, 21 µm, and occupy a planar area of approximately 0.7 × 0.7 mm.

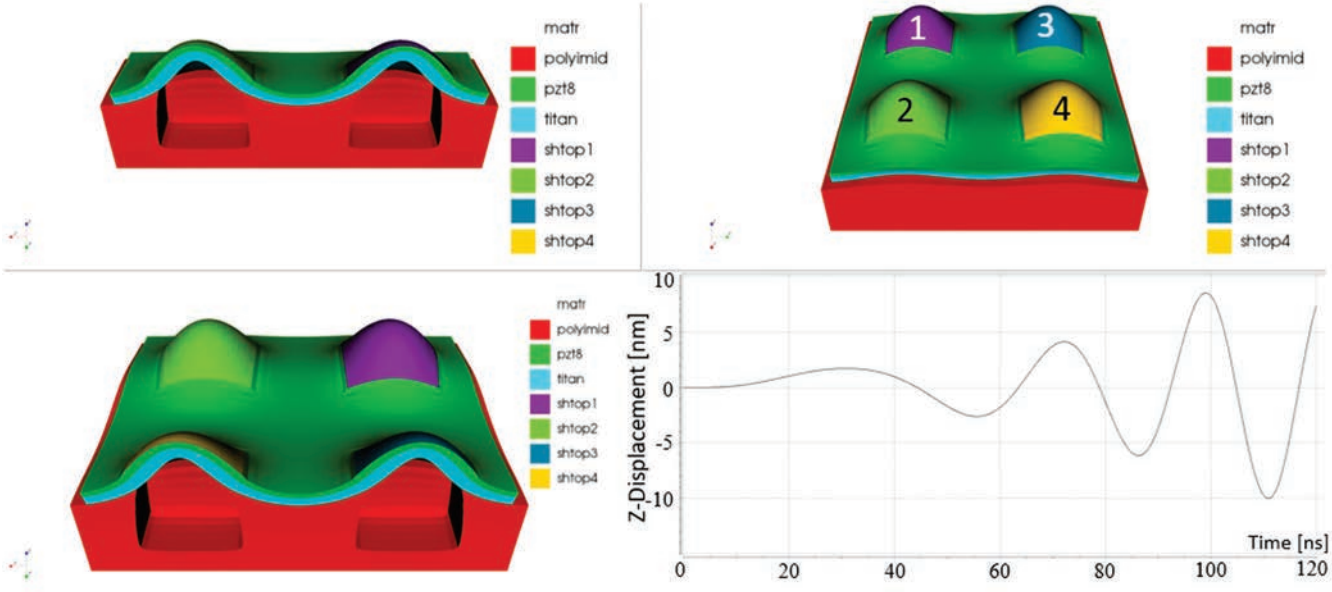

Fig. 3 — Snapshot of the quad diaphragm PMUT cell model running in vacuum for the electrical input impedance calculation.

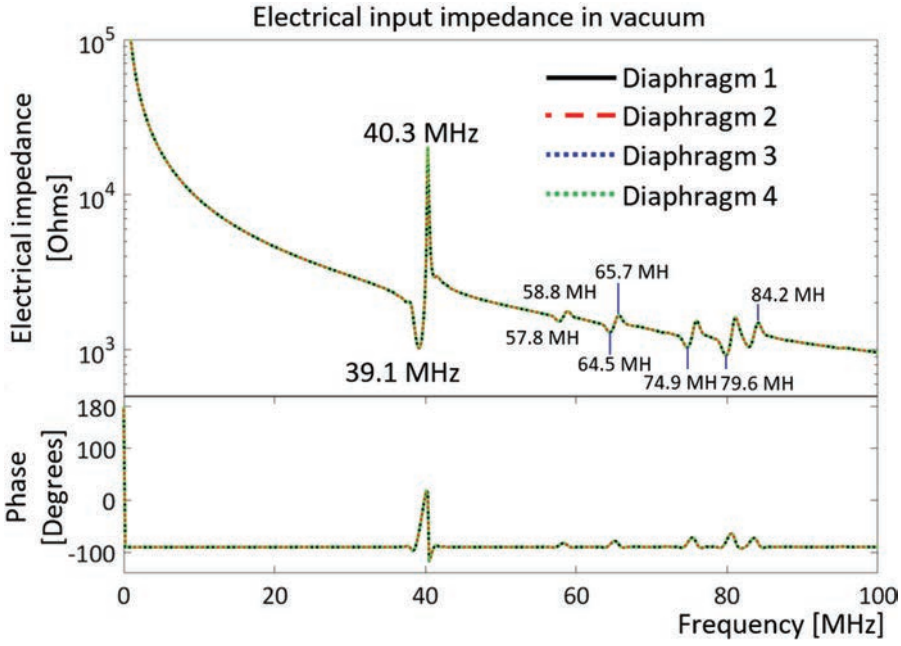

Fig. 4 — Electrical input impedance of the four diaphragms in the PMUT cell.

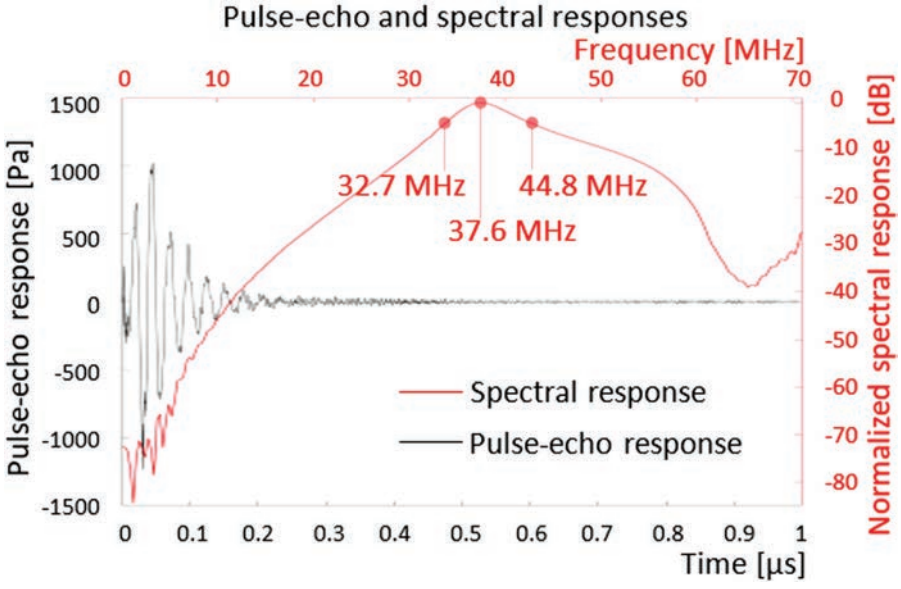

Fig. 5 — Pulse-echo and normalized spectral responses of the quad diaphragm PMUT cell model.

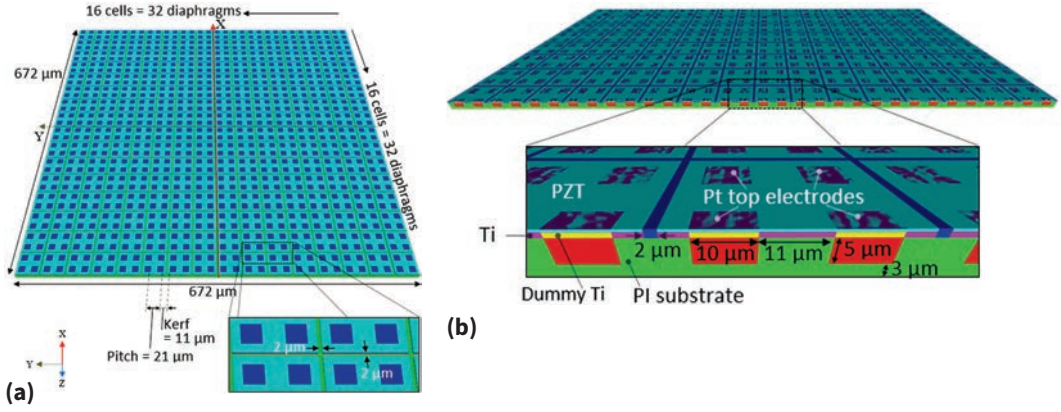

Fig. 6 — A 32×32 array model consisting of 256 (16×16) quad diaphragm PMUT cells in (a) angled planar view and (b) cross-section view.

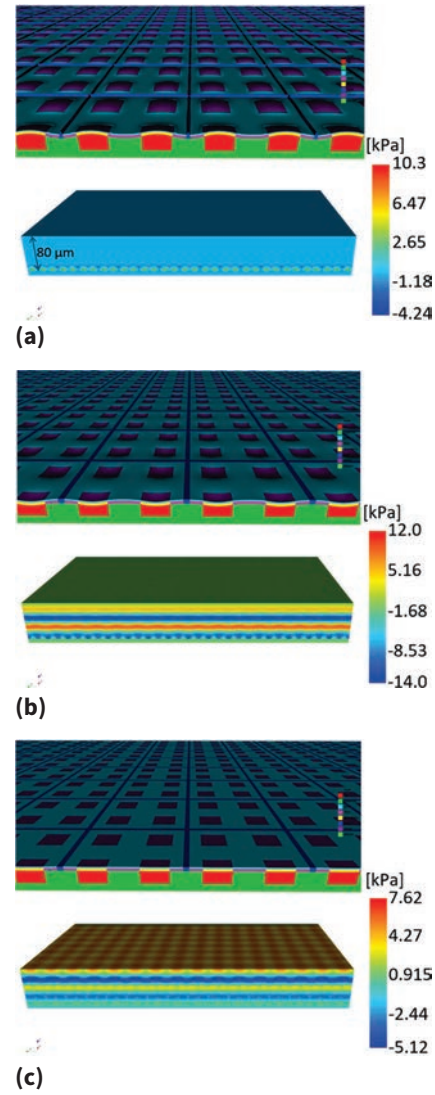

Fig. 7 — Diaphragm motion and acoustic wave propagation of the 32×32 array model at (a) 13.3 ns, (b) 60 ns, and (c) 0.12 μs.

Figure 7 illustrates snapshots of the diaphragm motions and acoustic pressure waves forming and propagating in water (25°C) at (a) 13.3 ns, (b) 60 ns, and (c) 0.12 μs, driven simultaneously by a 3 Vpp bipolar peak-to-peak voltage and 37.6 MHz single cycle sine wave.

In Fig. 7a, all the diaphragms moved upward together, with each diaphragm forming a spherical acoustic wave at 13.3 ns. In Fig. 7b, at 60 ns, four plane wave fronts were observed. Because the 80 μm water load was approximately two wavelengths in

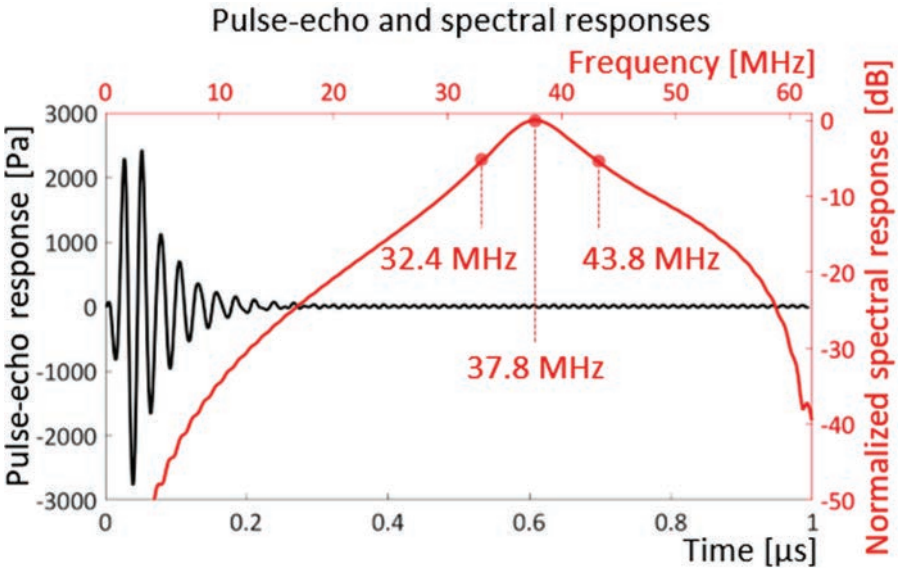

Fig. 8 — Pulse-echo and normalized spectral responses of the 32×32 array model.

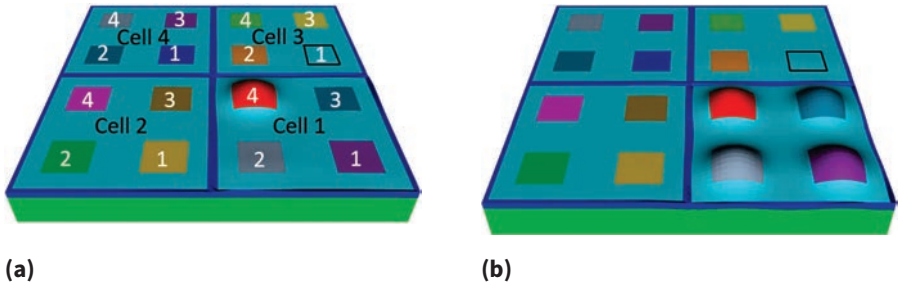

Fig. 9 — Two driving cases of the array model for crosstalk profiling, (a) single diaphragm and (b) single cell driven.

thickness (78 μm = 2 × 1500 m/s ÷ 37.6 MHz), the appearance of four wave fronts, which is the equivalent of 2 wave cycles, was reasonable. Figure 7c shows that the acoustic waves continued to be launched, propagated through the water, and reached the top of the water load. Figure 8 displays the pulse-echo and spectral responses of the 32×32 array model from this simulation.

The center frequency of the 2D array was 37.8 MHz and -6 dB frequency points were found at 32.4 MHz and 43.8 MHz, giving 30% bandwidth, as shown in Fig. 8. This array bandwidth well preserved the 32.3% bandwidth of the PMUT single cell model. In the time-domain, the pulse-echo response gave a clearer signal than those reported by Kim et al.[8]. This was attributed to a greater area of the 32×32 array being covered by PZT thin films, which are stiffer (26.5 to 115.4 GPa) than PI (8.5 GPa)[13]. Consequently, the PZT stiffness compensated for the compliance of the PI substrate, giving a clearer signal with less oscillation decay time while preserving the bandwidth.

Crosstalk profiling discovers unwanted cell to cell interference, which may degrade the performance of an array transducer. To determine cross-talk

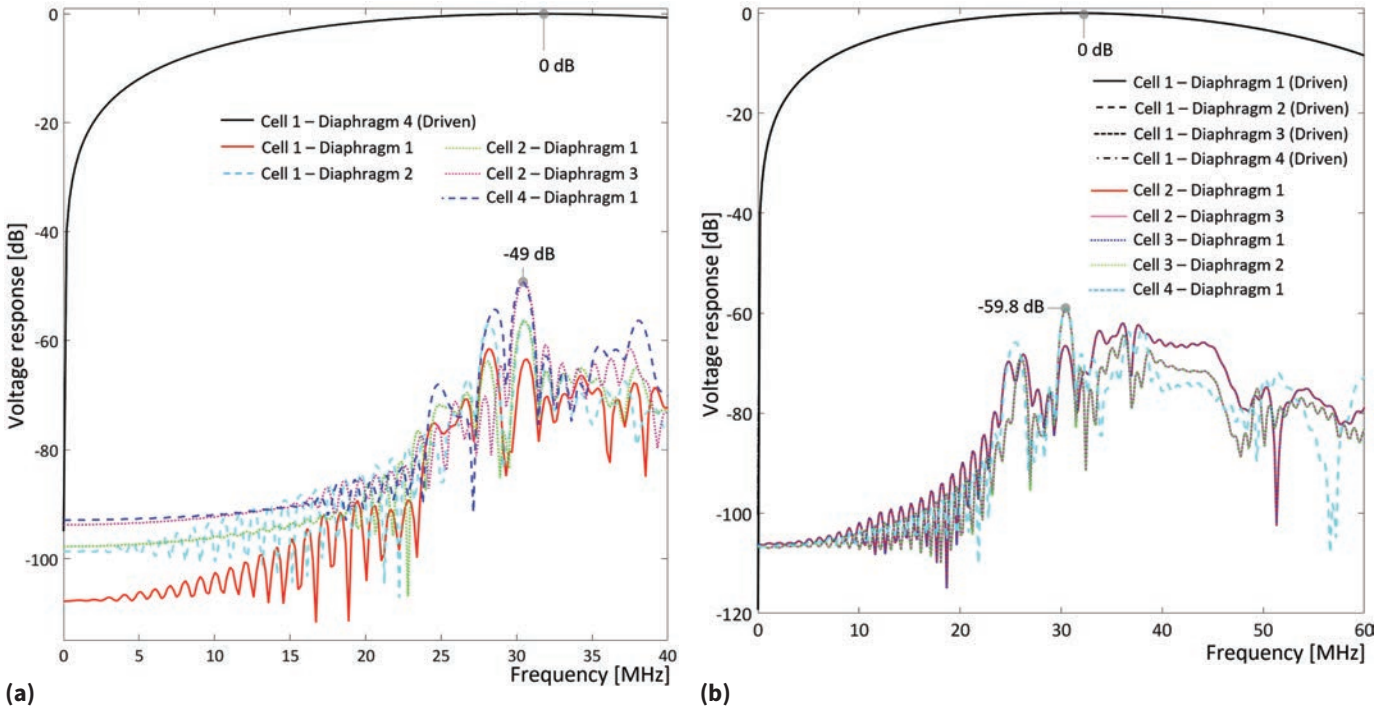

Fig. 10 — Crosstalk profiles of the array in two driving cases – (a) single diaphragm, and (b) single cell driven.

profiles, the array model was reduced to a 4×4 array for calculation efficiency. Two driving scenarios, single diaphragm driven and single cell driven, were considered. Figure 9 shows the 4×4 array models for these two driving cases in the crosstalk profile study.

In Fig. 9a, diaphragm 4 in cell 1 was driven, and in Fig. 9b the whole cell 1 was driven, and their adjacent diaphragms were monitored in terms of voltage response. Figure 10 displays the voltage responses of the equally distant diaphragms in the two cases.

In Fig. 10a the single diaphragm driven case does not reveal any patterns in the plot, while in Fig. 10b the single cell driven case shows the same voltage responses of the cells that have the same distances from the driven cell, cell 1. Diaphragm 1 in cell 2 and diaphragm 1 in cell 3 have the same response curves, and diaphragm 3 in cell 2 and diaphragm 2 in cell 3 show the same response plots. Furthermore, the single cell driven case has less maximum crosstalk, -59.8 dB, than that of the single diaphragm case, -49 dB. The results suggest that the quad diaphragm PMUT cell-based 2D array will be more stable when driven by cells rather than diaphragms.

CONCLUSION

This article discussed how a FEA approach could improve designs for robust and practical PMUT sensor array construction. PMUT array performance characteristics beyond those discussed in this article can determine: undesirable PMUT modal distortions; 3D beam profiles, depth of field and sharpness of acoustic wave propagation; and quantitative surface displacement profiles to ensure uniformity of diaphragm motions. The integration of design optimization with micro/nano fabrication technologies will have a major impact on the development of PMUT sensor array technologies for a broad spectrum of industrial and medical applications. **~AM&P**

For more information: Judith A. Todd, FASM, chair and professor, Department of Engineering Science and Mechanics, The Pennsylvania State University, University Park, PA 16802, jtodd@psu.edu.

Note: To see animation of the diaphragm deflections at their centers in the PMUT model simulation from Fig. 3, visit bit.ly/329e1Ch. To see animation of the diaphragm motions and acoustic pressure waves forming and propagating in water from Fig. 7, visit bit.ly/3mPzcRM.

References

1. https://www.qualcomm.com/products/features/fingerprint-sensors.

2. Y. Lu, et al., MUT Fingerprint ID System, U.S. Patent 10,430,631, issued October 1, 2019.

3. https://www.ultrasensesys.com/.

4. H.-Y. Tang, et al., Ultrasonic Touch Feature Extraction, U.S. Patent 10,585,534, issued March 10, 2020.

5. F. Griggio, et al., Micromachined Diaphragm Transducers for Miniaturised Ultrasound Arrays, 2012 IEEE International Ultrasonics Symposium, p 1-4, 2012, DOI: 10.1109 ULTSYM. 2012.0503.

6. T. Liu, et al., High-temperature Crystallized Thin-film PZT on Thin Polyimide Substrates, *J. Appl. Phys.,* 122(16), [164103], 2017. DOI: 10.1063/1.4990052.

7. C. Cheng, et al., Thin Film PZT-Based PMUT Arrays for Deterministic Particle Manipulation, *IEEE Transactions on Ultrasonics, Ferroelectrics, and Frequency Control,* 66(10), p 1605-1615, 8753665, 2019, DOI: 10.1109/TUFFC.2019.2926211.

8. J.N. Kim, et al., 10 MHz Thin-Film PZT-Based Flexible PMUT Array: Finite Element Design and Characterization, *Sensors,* 20(15), 4335, 2020.

9. I.K. Park, et al., Application of Flexible PAUT Probe for Weld Inspection of Piping Elbows, *Nondestructive Characterization and Monitoring of Advanced Materials, Aerospace, Civil Infrastructure, and Transportation XIII*, 10971, p 109711V, International Society for Optics and Photonics, 2019.

10. H. Zhou, et al., Stretchable Piezoelectric Energy Harvesters and Self-Powered Sensors for Wearable and Implantable Devices, *Biosensors and Bioelectronics,* 168(112569), 2020.

11. R. Talish and A. Winder, Ultrasound Bandage, U.S. Patent Application 11/799,355, filed September 6, 2007.

12. PZFlex 2018 embedded database, OnScale, 770 Marshall St. Suite 200 Redwood City, CA 94063.

13. PI-2600 Series – Low Stress Application, Product Bulletin, HD Micro-Systems, 250 Cheesequake Road, 703 Parlin, NJ.

14. S. Trolier-McKinstry and P. Muralt, Thin Film Piezoelectrics for MEMS, *J. Electroceram.,* 12(1-2), p 7-17, 2004.